SCIENCE CHINA
Earth Sciences

•ARTICLE•

https://doi.org/10.1007/s11430-025-1668-1

Improve the forecast reliability of unusual tropical cyclone tracks using ensemble forecasts generated by O-CNOPs

Han ZHANG[1,2,6], Wansuo DUAN[2*], Yongjie HUANG[3], Pak Wai CHAN[4] & Stephane VANNITSEM[5]

[1] *Henan Key Laboratory of Agrometeorological Support and Applied Technique, China Meteorological Administration (CMA), Zhengzhou 450003, China*
[2] *State Key Laboratory of Earth System Numerical Modeling and Application, Institute of Atmospheric Physics, Chinese Academy of Sciences, Beijing 100029, China*
[3] *Center for Analysis and Prediction of Storms and School of Meteorology University of Oklahoma, Norman Oklahoma 73072, USA*
[4] *Hong Kong Observatory, Hong Kong 999077, China*
[5] *Royal Meteorological Institute of Belgium, Brussels 1180, Belgium*
[6] *Henan Meteorological Observatory, Zhengzhou 450003, China*

Received April 9, 2025; revised August 4, 2025; accepted August 19, 2025; published online October 16, 2025

Abstract There exist significant challenges in accurately predicting unusual tropical cyclone (TC) tracks. This study applies the orthogonal conditional nonlinear optimal perturbations (O-CNOPs) method to the Weather Research and Forecast (WRF) model to improve ensemble forecast reliability of unusual TC tracks. Ensemble forecast experiments were conducted for twenty-three forecast periods of five TCs, all of which exhibited sharp turns, to examine the effectiveness of O-CNOPs. Results demonstrate that the O-CNOPs method outperforms the singular vectors (SVs) and bred vectors (BVs) methods by providing more stable and reliable improvements in TC track forecasting skills, from both deterministic and probabilistic perspectives. Notably, the O-CNOPs shows a superior ability to generate ensemble members that accurately predict the sharp turns of TCs at lead times from one to five days. These results highlight the superiority of the O-CNOPs method over the SVs and BVs methods in enhancing the forecasting accuracy of TC tracks, particularly for forecasting unusual TC tracks. This study underscores the potential of O-CNOPs to be extended to real-time TC forecasting and to play an important role in operational track forecasts.

Keywords Tropical cyclone, Ensemble forecast, Optimal perturbation

Citation: Zhang H, Duan W, Huang Y, Chan P W, Vannitsem S. 2025. Improve the forecast reliability of unusual tropical cyclone tracks using ensemble forecasts generated by O-CNOPs. Science China Earth Sciences, 68, https://doi.org/10.1007/s11430-025-1668-1

1. Introduction

Tropical cyclones (TCs) that occur over the western North Pacific (WNP) frequently bring extreme winds and heavy rainfall to China and pose significant threats to lives and property (Li and Zhao, 2022). The accuracy of TC-related wind and rainfall forecasts largely depends on the accuracy of TC track forecasts (Conroy et al., 2023; Qian et al., 2024). Therefore, a precise TC track forecast is essential to mitigate the severe impacts of TC-related disasters.

Over the past few decades, significant advancements have been made in TC track forecasting. However, substantial challenges remain in both long-time forecasts of TC tracks and the prediction of unusual TC tracks. Long-time forecasting of abnormal TC tracks is particularly difficult (Zhang et al., 2018; Chen et al., 2020; Tang et al., 2021; Li et al., 2023; Liu et al., 2024). Notably, in recent years, the frequent occurrence of TCs with unusual tracks over the WNP has

* Corresponding author (email: duanws@lasg.iap.ac.cn)

posed even greater challenges to operational TC forecasts. For instance, most meteorological services failed to forecast the sharp northward turn of TC In-Fa (2021) three days before TC turning. Even when initialized at the time approaching the turn, some forecasting centers still missed the turn, resulting in track errors significantly exceeding the annual-mean track error for the year 2021 (Xiang et al., 2022; Liu et al., 2024). Similarly, during the early stages of TC Khanun (2023), the leading meteorological services, such as the European Centre for Medium-Range Weather Forecasts (ECMWF) and the US National Centers for Environmental Prediction (NCEP), consistently predicted that the storm would make landfall in China (Nie et al., 2025). However, the cyclone abruptly turned sharply northeastward, avoiding China entirely. It was then predicted to strike Japan but unexpectedly shifted northward again, ultimately making landfall in the Republic of Korea. Another example is TC Saola (2023). Most meteorological services did not accurately forecast the loop at the early stage of the TC, causing prominent errors in the predicted landfall location. These examples highlight that the long-time forecasts generally struggle to replicate the unusual TC tracks. Even when forecasts are initialized close to the time of turning, they still exhibit very large forecast uncertainties regarding TC tracks.

Ensemble forecasting has been widely adopted by Meteorological Departments to improve TC forecasting skill, provide the information of forecast uncertainty, and generate probabilistic forecasts (Puri et al., 2001; Dube et al., 2020). Advances in ensemble forecasting methods have significantly enhanced TC forecasting skill (Duan et al., 2018; Zhang et al., 2023). It is widely accepted that fast-growing initial perturbations, superimposed on control forecasts to represent initial uncertainties, are crucial for improving the reliability of ensemble forecasts (Toth and Kalnay, 1993, 1997; Palmer, 2019; Magnusson et al., 2019). Particularly, numerous studies have highlighted the role of environmental steering flows, which are sensitive to initial conditions, in modulating TC tracks (Yamaguchi and Majumdar, 2010; Wang and Ni, 2011; Miller and Zhang, 2019; Miyachi and Enomoto, 2021; Ma et al., 2022; Zhang et al., 2023). This sensitivity underscores the initial value problem of TC track forecasts. The ECMWF has adopted the singular vectors (SVs) method and the NCEP previously used the bred vectors (BVs) method to account for the initial uncertainties in TC track forecasting. Both methods aim to generate fast-growing initial perturbations that replicate the forecast error growth and encompass the forecast uncertainties, achieving great success in improving TC track forecasting skill (Cheung and Chan, 1999; Cheung, 2001; Yamaguchi et al., 2009; Yamaguchi and Majumdar, 2010; Diaconescu and Laprise, 2012; Palmer, 2019). However, limitations remain. The BVs, responsible for growth behavior of initial perturbations prior to forecast initialization, often fail to maintain large growth rates during longer forecast lead times. This limitation frequently results in insufficient ensemble spreads to encompass the actual trajectory of the cyclones (Chan and Li, 2005; Lang et al., 2012; Thanh et al., 2016; Zhang et al., 2023). On the other hand, although SVs represent a group of fast-growing initial perturbations on control forecasts, they are derived from linearized dynamics of atmosphere motions and could possibly underestimate the forecast uncertainty when nonlinearities are playing an important role (Puri et al., 2001; Lang et al., 2012; Huo et al., 2019; Zhang et al., 2023).

Duan and Huo (2016) generalized SVs to the nonlinear regime and proposed the orthogonal conditional nonlinear optimal perturbations (O-CNOPs) method to fully account for the influence of nonlinearities. O-CNOPs represent a set of mutually orthogonal initial perturbations that have the maximum nonlinear evolution in their respective subspaces within a finite time interval (Duan and Huo, 2016; Huo et al., 2019; Zhang et al., 2023). Duan and Huo (2016) adopted a simple Lorenz-96 model (Lorenz, 1996) to address the dynamic rationality of the O-CNOPs and showed a significantly higher ensemble forecasting skill for the O-CNOPs than that of the SVs. Furthermore, Huo et al. (2019) extended the O-CNOPs to TC track ensemble forecasting using the fifth-generation Pennsylvania State University, National Center for Atmospheric Research Mesoscale Model (MM5) and showed clear advantages of O-CNOPs over methods based on random perturbations (RPs), BVs, and SVs. Although the MM5 model is generally considered less advanced and performs poorly in TC track simulations compared to the Weather Research and Forecasting (WRF) model (Pattanayak and Mohanty, 2008), subsequent studies reaffirmed the strength of O-CNOPs. Zhang et al. (2023) applied the O-CNOPs to TC track ensemble forecasting using the WRF model and found that the method consistently outperformed both the SVs and BVs methods, demonstrating superior deterministic and probabilistic forecasting skill. These findings underscore the significant potential of O-CNOPs for further improving TC track forecasting accuracy, making it a promising tool for operational meteorological applications.

As discussed above, long-time forecasts of unusual TC tracks remain particularly challenging, and so far, the capability of O-CNOPs in forecasting such unusual tracks has not been systematically evaluated. This raises a key question: can the O-CNOPs method greatly improve the accuracy of forecasting unusual TC tracks? To address this, the present study employs the O-CNOPs method to conduct ensemble forecasting experiments particularly for unusual TC tracks using the WRF model.

The rest of the paper is organized as follows. Section 2 describes the O-CNOPs method. Section 3 provides an overview of the TC cases with unusual tracks adopted in this study, along with an evaluation of the ensemble forecasting

performance achieved using the O-CNOPs, SVs, and BVs methods, and then details why the O-CNOPs is prone to capture the sharp turns of TC tracks. Finally, Section 4 provides the summary and discussion.

2. The O-CNOPs method and associated numerical model

In this study, we employ the O-CNOPs method within the WRFV3.6 model (Skamarock et al., 2008) to generate ensemble members for forecasting unusual TC tracks. Although our previous study (Zhang et al., 2023) also utilized WRFV3.6 and O-CNOPs for TC track forecasts, its focus was not on unusual tracks. Building on that, we continue to use WRFV3.6 but apply the O-CNOPs approach in a different manner, specifically tailored to forecasting unusual TC tracks. To avoid redundancy, we do not elaborate on the WRFV3.6 model here, as its details can be found in Zhang et al. (2023). Instead, we only present the specifics of our O-CNOPs implementation below.

The O-CNOPs, denoted as $\mathbf{x}_{0j}^{*}$ (j=1, 2, 3, ...), constitute a set of distinct initial perturbations that are mutually orthogonal and exhibit maximal nonlinear growth within a predefined time interval [0, τ], referred to as the "optimization time interval" (OTI; see Zhang et al., 2023), in their respective constrained subspaces Ω_j (Duan and Huo, 2016). The jth CNOP is obtained by solving the optimization problem given in eq. (1).

$$\mathbf{J}\left(x_{0j}^{*}\right)=\max_{x_{0j}\in\Omega_j}\left[PM_{\tau}\left(\mathbf{X}_0+\mathbf{x}_{0j}\right)-PM_{\tau}(\mathbf{X}_0)\right]^{\mathrm{T}}\times\mathbf{C}_2\left[PM_{\tau}\left(\mathbf{X}_0+\mathbf{x}_{0j}\right)-PM_{\tau}(\mathbf{X}_0)\right], \tag{1}$$

The subspace Ω_j is represented by

$$\Omega_j=\begin{cases}\left\{\mathbf{x}_{0j}\in\mathbf{R}^n\middle|\ \mathbf{x}_{0j}^{\mathrm{T}}\mathbf{C}_1\mathbf{x}_{0j}\leqslant\delta\right\}, & j=1,\\ \left\{\mathbf{x}_{0j}\in\mathbf{R}^n\middle|\ \mathbf{x}_{0j}^{\mathrm{T}}\mathbf{C}_1\mathbf{x}_{0j}\leqslant\delta,\mathbf{x}_{0j}\perp\Omega_k,k=1,\ldots,j-1\right\}, & j>1\end{cases} \tag{2}$$

where $\mathbf{X}_0\in\mathrm{R}^n$ represents the state vector, and M denotes the nonlinear propagator of the numerical forecast model. The superscript "T" indicates a transpose, and δ is a positive value defining the maximum allowable amplitude of the initial perturbation. The operator P serves as a local projection, taking a value of 1 when the final perturbations fall within the "verification region" (i.e., the region of interest for forecast accuracy) and 0 otherwise. In the current study, the verification region is defined as a fixed 10°×10° box centered on the TC position at the optimization time, a choice made to isolate the properties of the uncertainties in the TC circulation at this time (Tseng and Lai, 2020), while the initial perturbations are generated over the entire model domain. In eqs. (1) and (2), both C_1 and C_2 adopt the total moist energy and are expressed by eq. (3).

$$\|\delta\mathbf{X}\|_{C_1}^2=\|\delta\mathbf{X}\|_{C_2}^2=\frac{1}{D}\int_D\int_0^1\left[\mathbf{u}'^2+\mathbf{v}'^2+\left(\frac{g}{\overline{N}\,\overline{\theta}}\right)^2\boldsymbol{\theta}'^2+R_{\mathrm{a}}T_{\mathrm{r}}\left(\frac{\mathbf{p}'_s}{p_{\mathrm{r}}}\right)^2+\frac{L^2}{c_pT_r}\mathbf{q}'^2\right]\mathrm{d}\sigma\mathrm{d}D. \tag{3}$$

The eq. (3) involves the zonal wind perturbation ($\mathbf{u}'$), meridional wind perturbation ($\mathbf{v}'$), potential temperature perturbation ($\boldsymbol{\theta}'$), surface pressure perturbation ($\mathbf{p}'_s$), and water vapor mixing ratio perturbation ($\mathbf{q}'$). It also prescribes the physical reference temperatures $\overline{\theta}$=300 K, T_{r}=270 K, and pressure p_{r}=1000 hPa. In eq. (3), g represents the gravitational acceleration, R_{a} and c_p are the dry air gas constant and the constant-pressure specific heat of dry air, while $\overline{N}$ and L denote the Brunt-Vaisala frequency and the latent heat of condensation per unit mass, respectively. The vertical integrations of the kinetic and potential energy terms, associated with $\mathbf{u}'$, $\mathbf{v}'$, $\boldsymbol{\theta}'$ and $\mathbf{p}'_s$, extend up to the top level, while the water vapor term $\mathbf{q}'$ is limited to below 500 hPa.

Referring to Zhang et al. (2023), we choose the OTI=6 h, initial perturbation amplitude δ=1.8, and ensemble size N=21, for which the O-CNOPs ensemble achieves the highest ensemble forecasting skill for TC tracks. In this study, we still adopt the Spectral Projected Gradient 2 method (Birgin et al., 2000), as used in Zhang et al. (2023), to solve the optimization problem given by eq. (1) and compute the O-CNOPs. Since unusual TC motion may be influenced by multi-scale interactions, we employ a model domain with an increased resolution of 30 km horizontally and 31 vertical levels, extending from the surface to the top of the atmosphere at 50 hPa, for ensemble forecasting experiments in this study. In contrast to the approach used in Zhang et al. (2023), where O-CNOPs are calculated at a horizontal resolution of 60 km and 15 vertical levels, followed by ensemble forecasts at the same resolution, the present study first calculates the O-CNOPs at this coarser resolution and then linearly interpolates them to a higher resolution of 30 km horizontally and 31 vertical levels. The interpolated O-CNOPs are subsequently used to construct the initial perturbations for the actual ensemble forecasts. The ensemble size N=21 mentioned above requires 10 such initial perturbations. These initial perturbations, along with their negative counterparts, are then superimposed onto the initial field of the control forecast to generate 20 perturbed initial fields, with the control forecast utilizing the Global Forecast System (GFS) at 1.0°×1.0° resolution and 6-hour intervals to provide the initial and boundary conditions. The WRFV3.6 model with higher resolution is then integrated to generate 20 perturbed forecasts, which, along with the control forecast,

constitute 21 ensemble members for each case.

To assess the performance, the O-CNOPs ensemble forecasts are compared with those generated using traditional methods, including the SVs method implemented in the ECMWF and the BVs method previously used by NCEP. The configurations for both the SVs and BVs are identical to those employed in Zhang et al. (2023), where it was shown that O-CNOPs achieves higher forecasting skill than both SVs and BVs under various configurations. A brief overview of the SVs and BVs methods was provided in Appendix A of Zhang et al. (2023).

3. Ensemble forecasts for unusual TC tracks

In this section, we first describe the TCs with unusual tracks, and then assess the ability of O-CNOPs to improve the ensemble forecasting skill of unusual tracks compared with SVs and BVs.

3.1 Cases overview

To explore the ensemble forecasts of unusual tracks, it is necessary to distinguish unusual TC tracks from typical ones. However, a universally accepted definition of sudden TC track changes has not yet been established (Li et al., 2023). In operational forecasting in China, thresholds of a 45° right deflection or a 30° left deflection within 12 h are commonly used to identify unusual TC tracks. These criteria have also been used in previous studies, such as Gong et al. (2018). Interestingly, Dai et al. (2014) provided the rationale behind the above criteria, illustrating that in the WNP, the occurrence probability of a right deflection exceeding 45° within 12 h is less than 2.8% and that of a left deflection exceeding 30° is less than 8.7%. These criteria effectively identify sharp turning tracks, distinguishing them from gradually recurving ones. Besides, we do not consider the short fluctuations around a relatively smooth track, so the TC's movements should be relatively stable after passing the turning point. Based on these criteria, we select three TCs exhibiting unusual tracks (i.e., Hinnamnor (2022), Khanun (2023), Saola (2023)) from 2022 to 2023. Additionally, Megi (2010) and Tembin (2012), previously analyzed in Zhang et al. (2023) without a focus on unusual tracks, also satisfy these criteria and are included in this study. All five TCs had significant impacts on China.

The tracks of these five TCs are shown in Figure 1, which highlights six sharp turning points (as marked by red stars). Both Megi (2010) and Hinnamnor (2022) underwent an abrupt northward turn, while Khanun (2023) followed a zigzagging track with a sharp northeastward turn on 4 August 2023 and another abrupt northward turn on 7 August

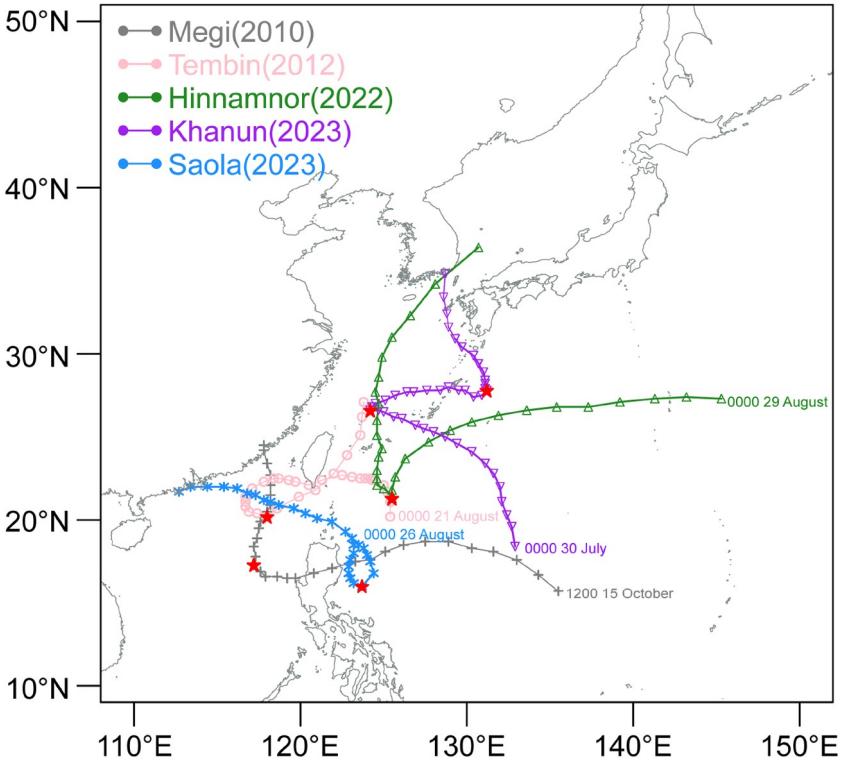

Figure 1 Best tracks of the five selected TCs(i.e., Megi (2010), Tembin (2012), Hinnamnor (2022), Khanun (2023), Saola (2023)) as obtained from the China Meteorological Administration (CMA). The starting points of each track correspond to their first initialized times, with subsequent tracks marked at 6-h intervals. The red stars denote six unusual turning points of the five TC case.

2023. Meanwhile, Tembin (2012) and Saola (2023) exhibited counterclockwise looping tracks. For the five TC cases, a total of eighteen forecast periods, detailed in Table 1, span between five and ten days, depending on each TC's lifetime. Since Khanun (2023) experienced two abrupt turns during its forecast periods, there are twenty-three ensemble forecast experiments for the six turning points.

3.2 Evaluation of ensemble forecasts for sharp TC turns

We conduct twenty-three ensemble forecast experiments for the six turning points of the five TCs, following the methodology outlined in section 2. Each forecast has 21 ensemble members, resulting in a total of 483 ensemble members generated for each method, i.e., the O-CNOPs, SVs, and BVs. Utilizing these ensemble members, we evaluate the probability of accurately capturing the sharp turns of the TCs. Additionally, the performance of ensemble mean forecast is also evaluated by quantifying the track errors during the turning stages. The results are analyzed and compared among the three methods.

Figures 2–4 show the control forecasts and the corresponding ensemble forecasts using BVs, SVs and O-CNOPs. The results reveal that the control forecasts significantly deviate from the best track, especially when initialized well before the TC turning timing. These forecasts frequently fail to accurately capture the timing, location, and angle of the TC turn. In this case, effective ensemble forecasts should adequately represent the uncertainty, allowing the true TC track to fall within the ensemble spread. However, as shown in Figures 2–4, the ensemble members made by BVs and SVs tend to closely cluster around the control forecasts, while the best tracks often fall outside the ensemble spread, particularly for longer lead times. Differently, O-CNOPs can provide more ensemble members that obviously deviate from the corresponding control forecasts and often exhibit a broader spread to cover the best tracks. Statistically, among the twenty-three forecasts, eighteen forecasts using O-CNOPs successfully span the best track with their turning locations, timing, and angles, while only five forecasts using SVs and four forecasts using BVs achieve this outcome (see Table 1). This implies that the O-CNOPs method has a significantly higher probability of capturing the sharp TC turns in forecasts compared to the SVs and BVs.

Now we quantify the probabilities of the ensemble members made by O-CNOPs capturing the sharp turn of TCs, including their turning location, timing, and angle. Such probabilistic assessments in real-world forecasts can provide useful warning information for decision-makers. To address

Table 1 Forecast periods (UTC) for each TC[a)]

TC names	Forecast periods (UTC)	O-CNOPs		SVs		BVs	
Megi	12:00 15 October 2010 to 12:00 23 October 2010	√		×		×	
	12:00 16 October 2010 to 12:00 23 October 2010	√		×		×	
	12:00 17 October 2010 to 12:00 23 October 2010	√		√		×	
	12:00 18 October 2010 to 12:00 23 October 2010	√		√		√	
Tembin	00:00 21 August 2012 to 00:00 29 August 2012	√		×		×	
	00:00 22 August 2012 to 00:00 29 August 2012	×		×		×	
	00:00 23 August 2012 to 00:00 29 August 2012	√		√		√	
Hinnamnor	00:00 29 August 2022 to 00:00 06 September 2022	×		×		×	
	00:00 30 August 2022 to 00:00 06 September 2022	√		×		×	
	00:00 31 August 2022 to 00:00 06 September 2022	√		√		√	
	00:00 01 September 2022 to 00:00 06 September 2022	√		×		×	
Khanun	00:00 30 July 2023 to 00:00 09 August 2023	√	×	×	×	×	×
	00:00 31 July 2023 to 00:00 10 August 2023	√	√	×	×	×	×
	00:00 01 August 2023 to 00:00 10 August 2023	√	×	×	×	×	×
	00:00 02 August 2023 to 00:00 10 August 2023	√	√	×	×	×	×
	00:00 03 August 2023 to 00:00 10 August 2023	√	√	√	×	√	×
Saola	00:00 26 August 2023 to 00:00 02 September 2023	×		×		×	
	00:00 27 August 2023 to 00:00 02 September 2023	√		×		×	

a) Check marks (√) indicate that the ensemble members for the O-CNOPs, SVs or BVs successfully encompass the best track including the turning location, time, and angle. Cross marks (×) indicate that the ensemble members fail to span these key turning features.

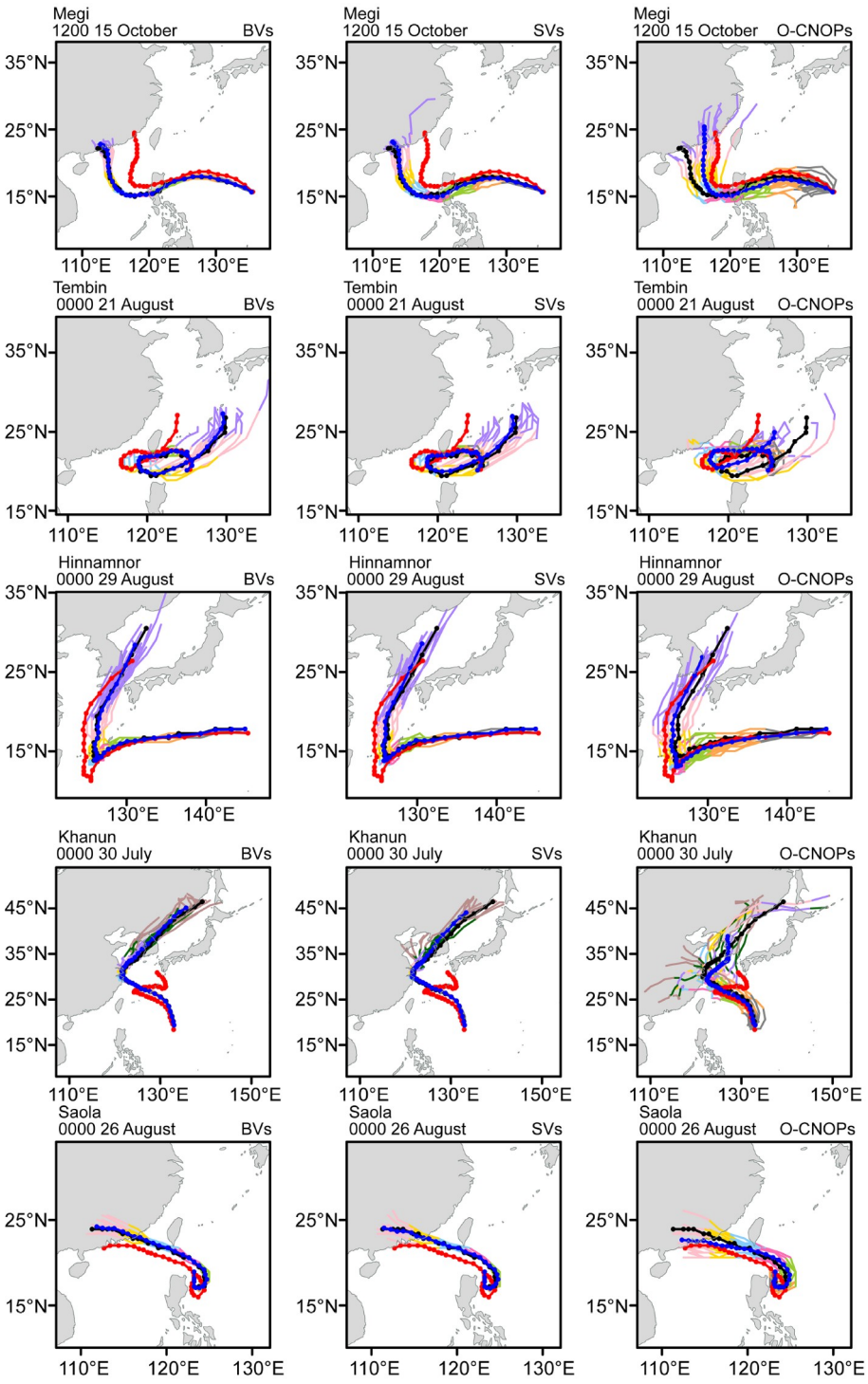

Figure 2 The ensemble forecasts of TC tracks during the first forecast periods of Megi (2010), Tembin (2012), Hinnamnor (2022), Khanun (2023) and Saola (2023) generated by the BVs (left column), SVs (middle column), and O-CNOPs (right column). Here are the best tracks (red lines), control forecasts (black lines), ensemble mean forecasts (blue lines) and the ensemble member forecasts. Time phases marked with different colors represent 0–24 h (gray lines), 24–48 h (orange lines), 48–72 h (green lines), 72–96 h (magenta lines), 96–120 h (light blue lines), 120–144 h (yellow lines), 144–168 h (pink lines) and 168–192 h (purple lines), 192–216 h (dark green lines), and 216–240 h (brown lines).

this question, we define allowable error bounds for forecast accuracy in predicting the sharp turn components (turning location, time, and angle). This unusual approach has been designed since there is no standardized metric for TC turning forecast accuracy. The different combinations of error bounds in Table 2 produce a total of twenty-seven categories of distinct degrees of accuracy for evaluating TC turning forecasts. In Figure 5, the percentage of the number of en-

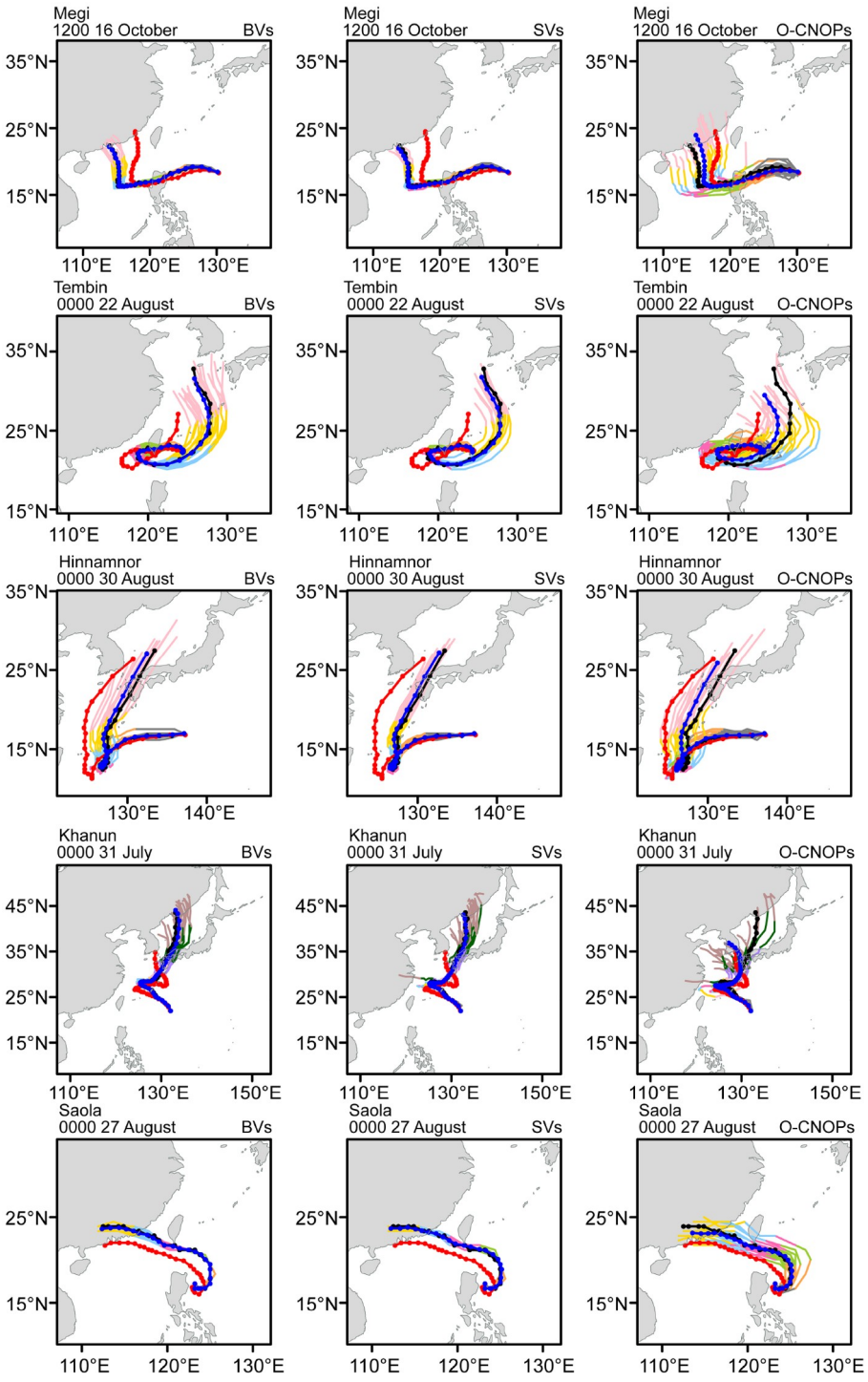

Figure 3 Same as Figure 2, but for the tracks in the second forecast periods of Megi (2010), Tembin (2012), Hinnamnor (2022), Khanun (2023) and Saola (2023).

semble members that capture the sharp TC turns among the 483 members generated from the 23 forecast experiments is plotted for each kind of degree of accuracy. It is shown that, across all degrees of accuracy, the percentages achieved by the O-CNOPs method, i.e. 10%–63%, are consistently and significantly higher than those obtained using SVs and BVs, i.e. 3%–38% and 2%–33%. It highlights the potential of O-CNOPs to provide more ensemble members that better capture the sharp turns of TCs and provide more reliable probabilistic information regarding the occurrence of sharp turns, which could enhance forecast guidance and decision-making.

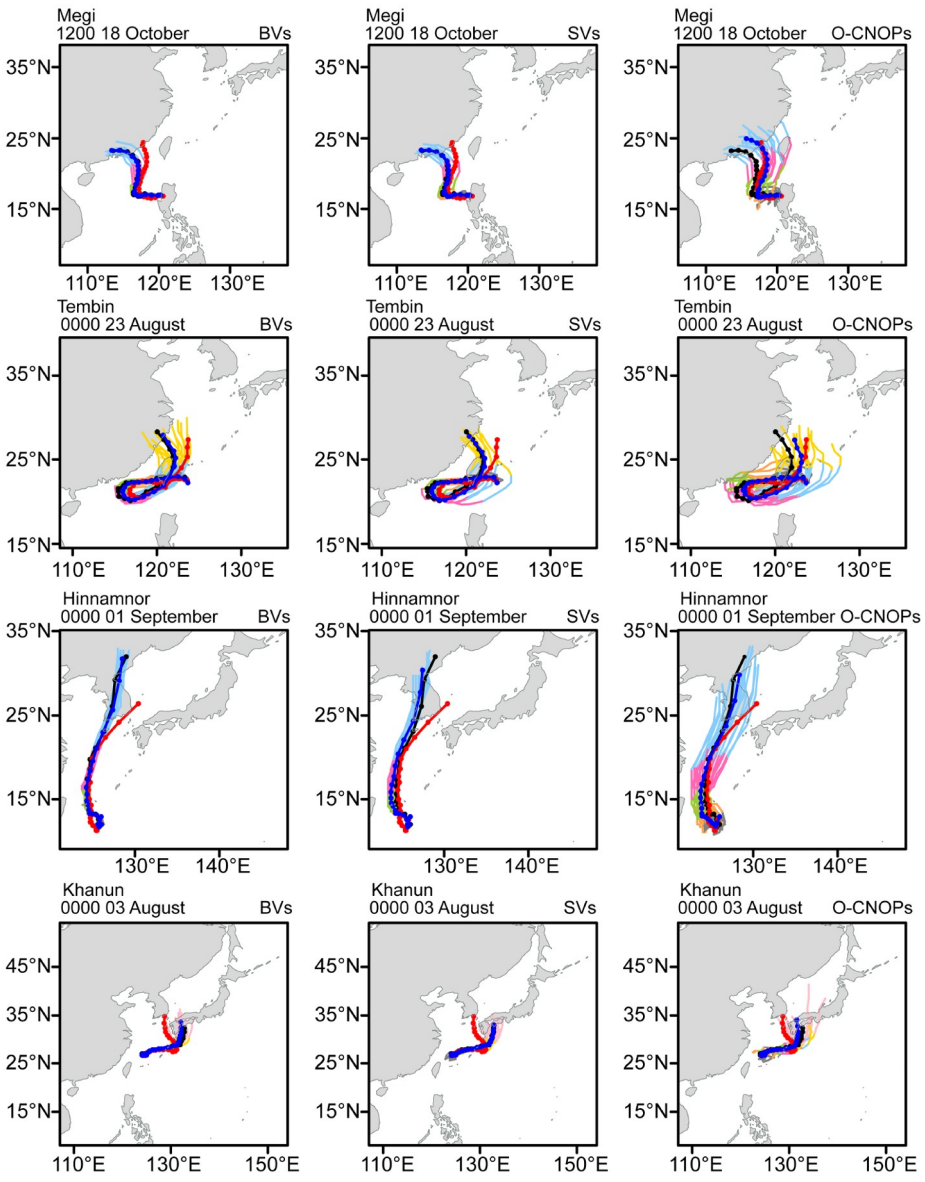

Figure 4 Same as Figure 2, but for the tracks in the last forecast periods of Megi (2010), Tembin (2012), Hinnamnor (2022) and Khanun (2023).

Figure 6 further provides the percentage of ensemble members that capture the sharp turn among the total ensemble members at lead times of 24, 48, 72, 96, and 120 h. These calculations assume allowable error bounds of 120 km for turning location, 12 hours for turning time, and 10° for turning angle. Note that the control forecasts of five TCs often only capture the turning time and location within the above allowable degree of accuracy for lead times of 1–2 days, but fail to accurately forecast the angle of deflection (see Figure 4). In contrast, from Figure 6, it is evident that the O-CNOPs produces more members capable of reproducing the sharp turn 1 to 5 days in advance compared to the SVs and BVs. Specifically, at lead times from 1 to 3 days, more than 50% of O-CNOPs ensemble members capture the sharp turns of these TCs. At a lead time of 4 days, nearly 50% of the O-CNOPs ensemble members succeed, and at a lead time of 5 days, more than 30% of the O-CNOPs ensemble members still capture the sharp turns. For the BVs and SVs, however, only at lead times of 1 and 2 days do more than 50% of the ensemble members successfully capture the sharp turns. Beyond 3 days, the percentages drop sharply, with less than 10% of ensemble members capturing the sharp turn at lead times of 4 and 5 days. This limitation significantly reduces their ability to provide advanced warning for TC track changes. Taking Khanun (2023) as an example, when initialized at five days prior to its first sharp turn, the control forecast and all members for the BVs and SVs erroneously predicted landfall along the southeastern coast of China. However, about 30% of the ensemble members for the O-CNOPs successfully predicted its sharp northeastward turn

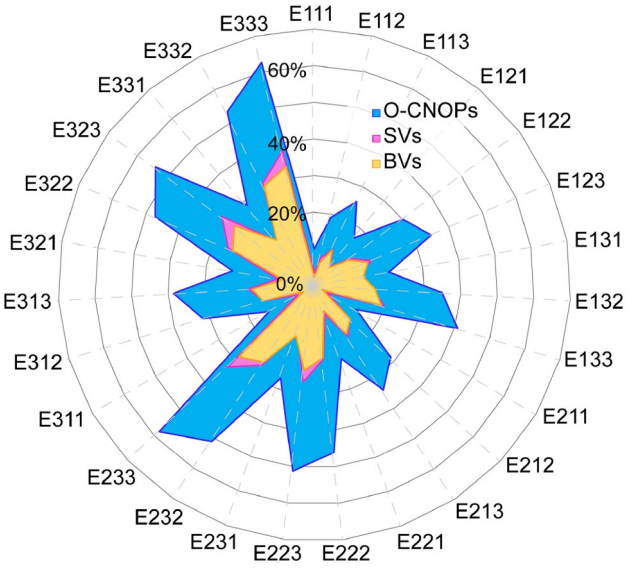

Figure 5 The percent of the number of the ensemble members capturing the TC turns among the total number of ensemble members for the twenty-three forecast periods (so a total of 483 forecasts). Yellow is for BVs, purple is for SVs, and blue is for O-CNOPs. The notation E*ijk* (*i*= 1, 2, 3; *j*=1, 2, 3; *k*=1, 2, 3) represents the category of the degrees of accuracy provided by *i*th error bound for turning location, *j*th error bound for turning time, and *k*th error bound for turning angle in Table 2.

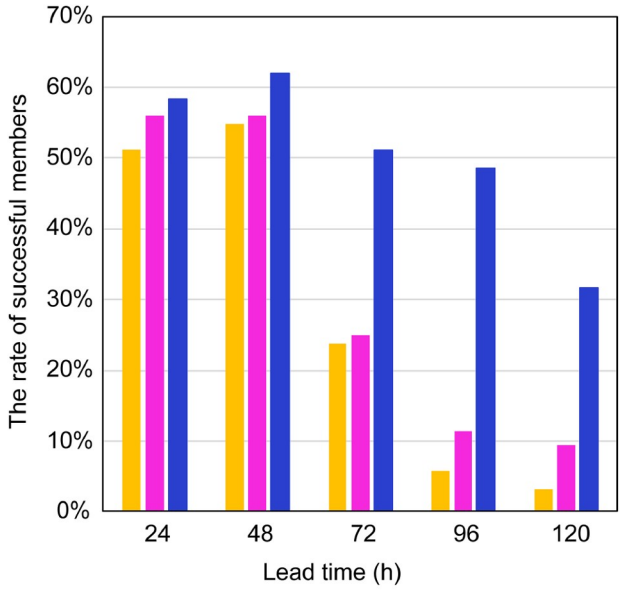

Figure 6 The percentage of ensemble members successfully capturing the TC sharp turns relative among the total number of ensemble members generated by O-CNOPs (blue), the SVs (purple), and the BVs (yellow) at different lead times when the degree of accuracy is prescribed by the following error bounds: 120 km for turning location, 12 h for turning timing, and 10° for turning angle.

Table 2 Error bounds for the forecast accuracy in predicting the timing, location, and angle of TC turn.

Error bounds	Turning location	Turing time	Turning angle
1	60 km	6 h	5°
2	120 km	12 h	10°
3	180 km	18 h	15°

(see Figure 2). Therefore, the O-CNOPs demonstrates a superior ability to generate more members that successfully predict the sharp turns of TCs at longer lead times, thereby offering more valuable warning information on the sudden changes of TC tracks.

We further quantify the deterministic skill of ensemble mean forecasts made by BVs, SVs, and O-CNOPs in forecasting the sharp turns of the TC tracks. Firstly, we compare the forecast errors of turning location and time among the control forecasts and three ensemble mean forecasts. As shown in Figure 7, the forecast errors of the turning location and time for the O-CNOPs ensemble mean forecast (152 km, 8 h) are smaller than those of the control forecast (225 km, 11 h). Particularly, O-CNOPs exhibit clear advantage over BVs and SVs in reducing large forecast errors related to the turning position and turning time. Although O-CNOPs show higher probabilistic skill in capturing the turning angle, the ensemble mean generated by O-CNOPs, as well as those for BVs and SVs, performs worse than the control forecast in forecasting the turning angle within 12 h. The sharp turning angles within 12 h of the ensemble mean forecasts are overly smoothed compared to each individual ensemble member due to filtering effects (see Figures 2–4). From another perspective, Qian and Mao (2023) computed the track errors during the turning stages to evaluate the forecasting skill for the sharp turns of the TC tracks. Building upon this approach, we also examine the ensemble mean forecast errors for TC tracks during the turning stages, starting 24 hours before and ending 24 hours after the turning time. The ensemble mean forecast errors of the twenty-three forecasts, together with the control forecasts, are presented in Figure 8 using box–whisker plots. It is shown that the track errors of control forecasts gradually increase as TCs approach their turning points. Ensemble mean forecasts for the BVs and SVs provide only minor improvements over the control forecasts, with error reduction rates of less than 3%. Notably, the ensemble mean forecasts using O-CNOPs significantly decrease track errors during sharp turns across all three quantiles (25th, 50th and 75th). Specifically, the O-CNOPs ensemble mean forecasts reduce the track errors of the control forecasts by over 29% on average across all twenty-three forecasts. For control forecasts with errors in the upper quartile (indicating relatively large track errors), O-CNOPs achieve error reductions exceeding 34%, whereas the reductions for SVs and BVs are less than 2%. Furthermore, the smallest interquartile range, defined as the difference between 25th and 75th quantiles, demonstrates that the O-CNOPs method provides more stable and consistent improvement to the control forecasts compared to the SVs and BVs methods.

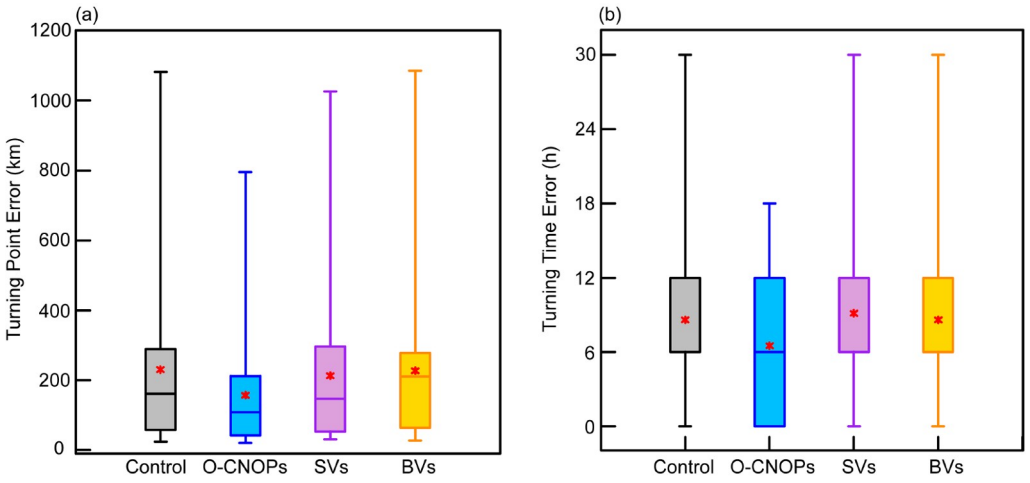

Figure 7 Box plots of the turning point errors (a) and turning time errors (b) for the twenty-three forecasts in the control forecasts (black) and ensemble mean forecasts using BVs (yellow), SVs (purple), and O-CNOPs (blue). The red points represent the mean values and the boxes show the 25th, 50th and 75th percentiles. The top and bottom lines indicate the largest and smallest values excluding outliers.

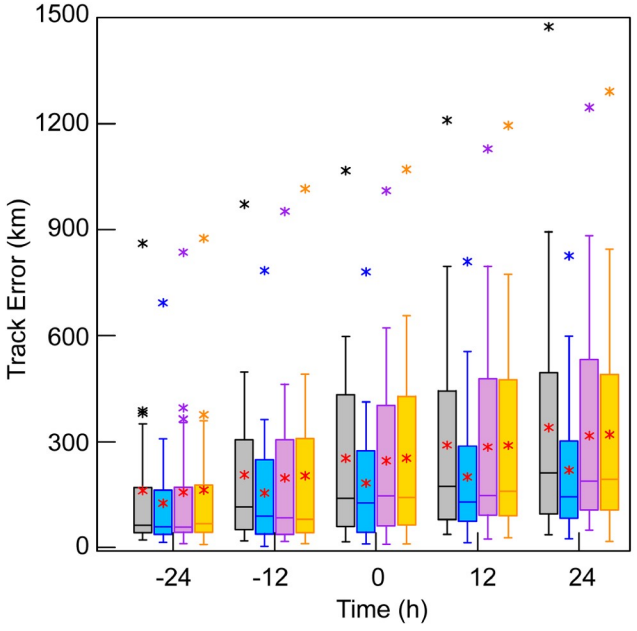

Figure 8 Box plots of track errors for the twenty-three forecasts during TC turning stage (defined as 24 h before to 24 h after the turning time) in the control forecasts (black) and ensemble mean forecasts using BVs (yellow), SVs (purple), and O-CNOPs (blue). The red points represent the mean values, the other points are the outliers, and the boxes show the 25th, 50th and 75th percentiles. The top and bottom lines indicate the largest and smallest values excluding outliers.

3.3 Explaining why the O-CNOPs ensemble members are more prone to capture TC sharp turn

Among the eighteen forecast periods in Table 1, the control forecast of Khanun (2023) has the largest track errors during its first forecast period, which was initialized at 00:00 UTC on 30 July 2023 (approximately 5 days prior to its sharp northeastward turn). As stated in Section 1, this sharp northeastward turn of Khanun (2023) also posed great challenges to operational forecasts. For such a difficult forecast case, only O-CNOPs ensemble is capable of generating ensemble members that noticeably deviate from the corresponding control forecasts and exhibit a broader spread to encompass the best track, thereby achieving better forecast reliability (see Figure 2). In the rest of this section, we take the forecast of Khanun (2023) initialized at 00:00 UTC on 30 July 2023 as an example to illustrate why O-CNOPs are more prone to generate ensemble members that capture the sharp northeastward turn of Khanun (2023), whereas both SVs and BVs fail to do so.

The perturbed total moist energies (TMEs) differ in vertical structures among the three methods (see Figure 9). The initial TMEs for BVs exhibit the largest magnitudes at the upper layers above 300 hPa, and the TMEs for SVs have the largest magnitudes in the low level below 800 hPa, while O-CNOPs have the largest TMEs in the middle to lower pressure levels, as illustrated in Zhang et al. (2023). Actually, the initial uncertainties in the middle to lower troposphere can lead to large forecast uncertainties of TC tracks (Wang and Ni, 2011; Torn et al., 2018). Notably, O-CNOPs are unique in effectively capturing this critical sensitivity. As a result, the sensitivity of O-CNOPs promotes a more significant amplification of TMEs across all vertical layers compared to SVs and BVs (see Figure 9). Consequently, O-CNOPs are more prone to generate ensemble members able to diverge more from the control forecast, which misses the sharp northeastward turn of Khanun (2023), thus producing a larger ensemble spread that has a superior ability to capture sharp turns of TC tracks (see Figure 2).

Figure 10 shows the horizontal structures for the first three BVs, SVs and O-CNOPs, along with the 500 hPa geopotential height and steering flow for the control forecast at the

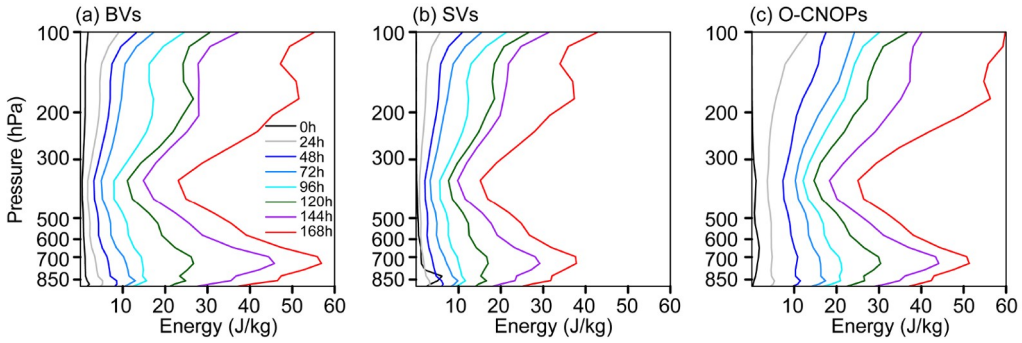

Figure 9 When initialized at 00:00 UTC on 30 July 2023 for TC Khanun (2023), vertical profiles of the TMEs (unit: J/kg) averaged over the entire analysis domain and across all ensemble members respectively generated by (a) BVs, (b) SVs and (c) O-CNOPs at the initial time (black curves) and at the lead times of 24 to 168 h (colored curves).

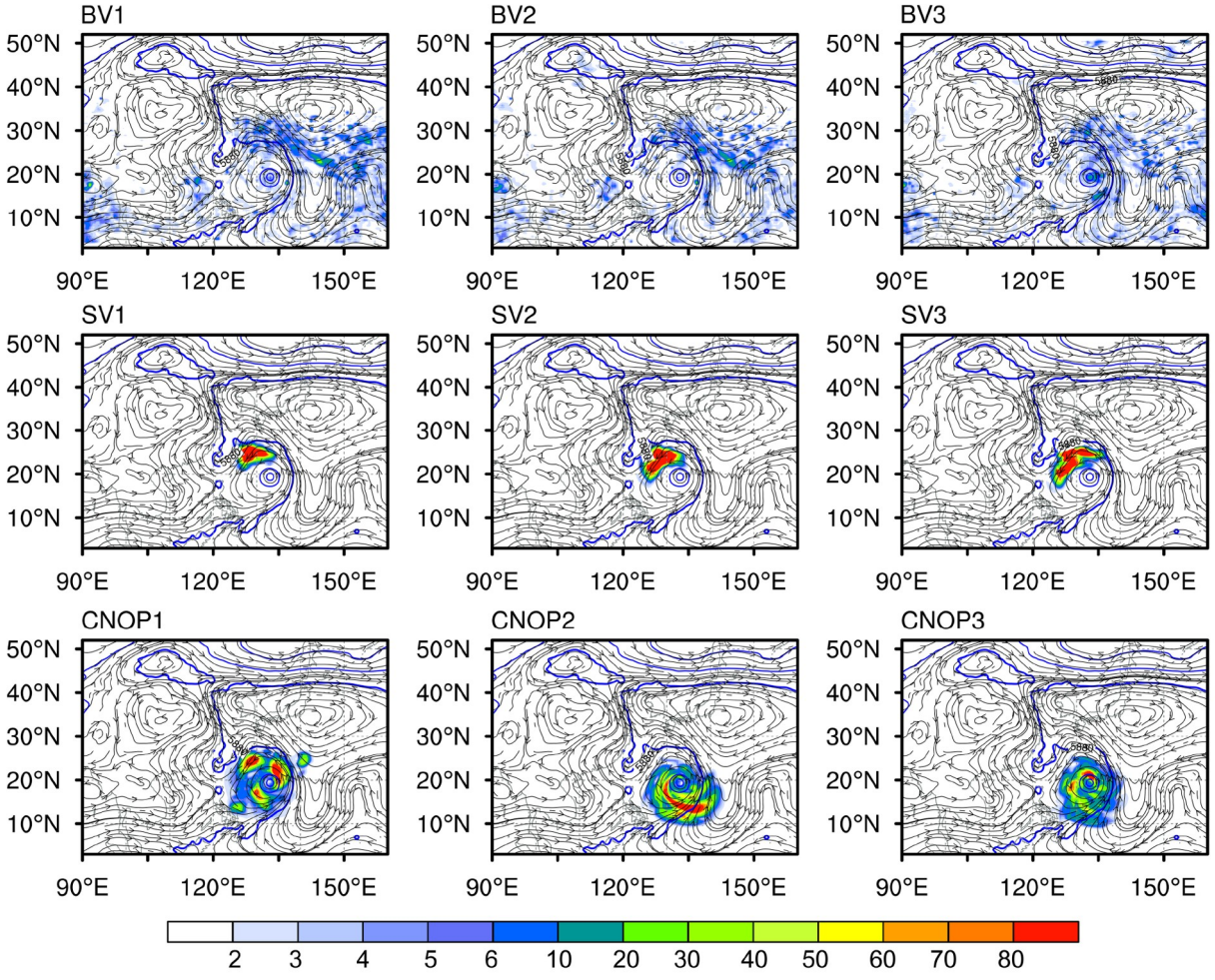

Figure 10 Horizontal structures of vertically averaged TMEs (shading; unit: J/kg) for the first three BVs, SVs and O-CNOPs. The blue contours and black streamlines show the 500 hPa geopotential heights (unit: gpm) and deep-layer (from 250 to 850 hPa) mean winds (unit: m/s).

initial time. It is known that Khanun (2023) initially moves northwestward due to the southeasterly steering flow associated with the western Pacific subtropical high (WPSH) and the subsequent unusual movement of Khanun (2023) is determined by the intensity and location changes of the WPSH (Chen et al., 2024). As is visible in Figure 10, the TMEs for BVs are scattered around the TC and its associated large-scale flows, while both SVs and CNOPs concentrate their TMEs in the confluence regions of the circulations represented by WPSH and Khanun (2023). However, their energy distributions differ: the SVs place their TMEs to the northwest of Khanun (2023), while O-CNOPs form a half-

annulus distribution around Khanun (2023). Both of them reflect the influence of WPSH on the TC, but the O-CNOPs ensemble provides a much larger spread than the SVs ensemble (and also the BVs ensemble) in the vicinity of Khanun (2023) and its surrounding steering flow at the initial stage (see Figure 11a). This broader spread is attributed to the fully nonlinear optimal growth nature of O-CNOPs. This would contribute to much larger alterations in the location and structure of Khanun (2023), which interact dynamically with the WPSH and further influence its intensity and location, in turn modulating the movement of the TC.

Figure 12 shows the 5880-gpm contour at 500 hPa for the three ensembles, outlining the structures of WPSH. The O-CNOPs ensemble displays much larger diversity in the intensity and location of WPSH (see Figure 12a), representing its larger uncertainties, especially as the forecast approaches the northeastward turn of Khanun (2023). This enhanced spread of WPSH is accompanied by a broader range of steering flows along its edge (see Figure 11a), which is critical in determining the TC's northeastward turn. As a result, the O-CNOPs ensemble generates substantial variability in the turning location and angle of its members (see Figure 2).

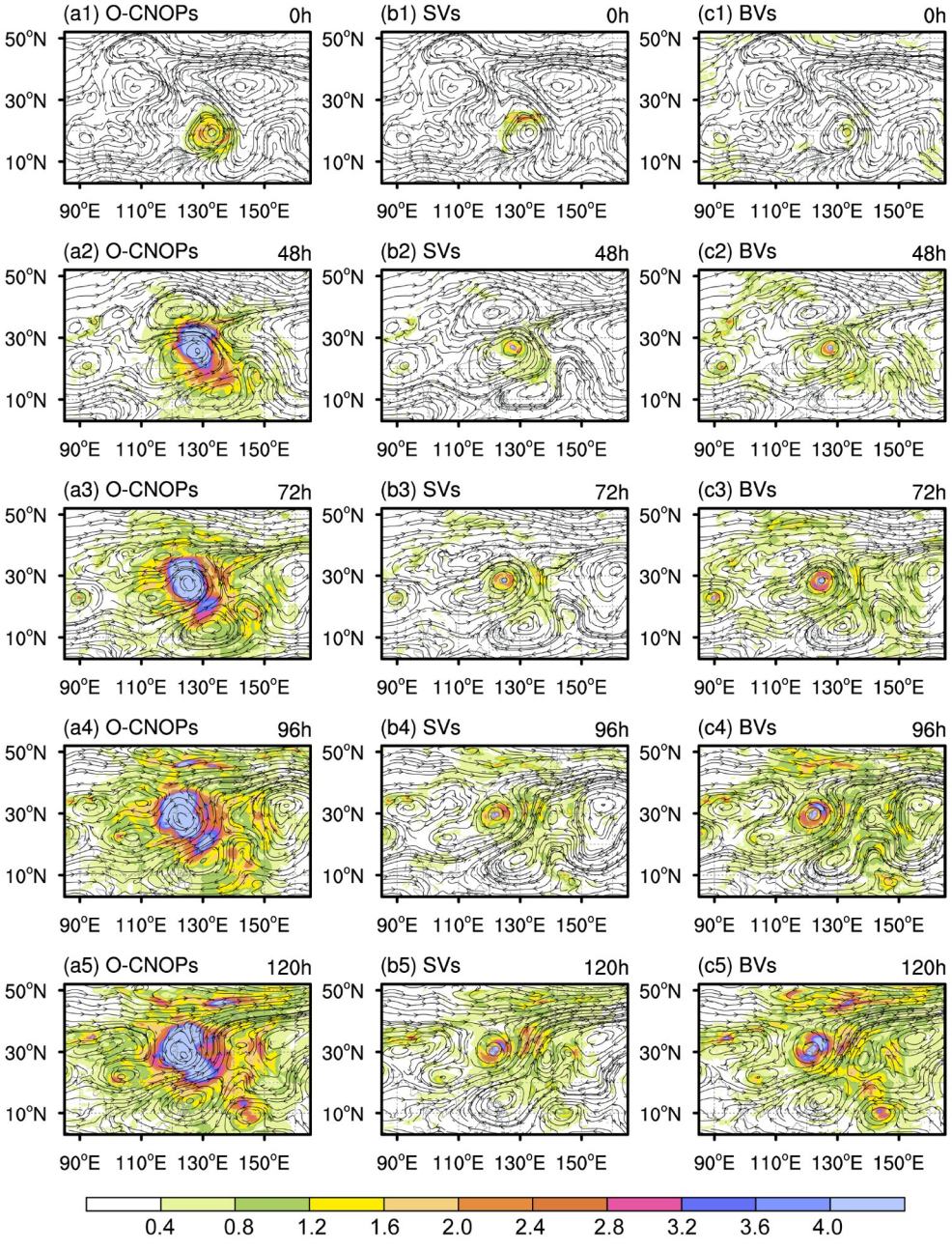

Figure 11 The black streamlines and shading respectively denote the ensemble mean and the corresponding ensemble spread of steering flow (unit: m/s) made by the O-CNOPs (a1–a5), SVs (b1–b5), and BVs (c1–c5) at the initial time and at the lead times of 48 to 120 h.

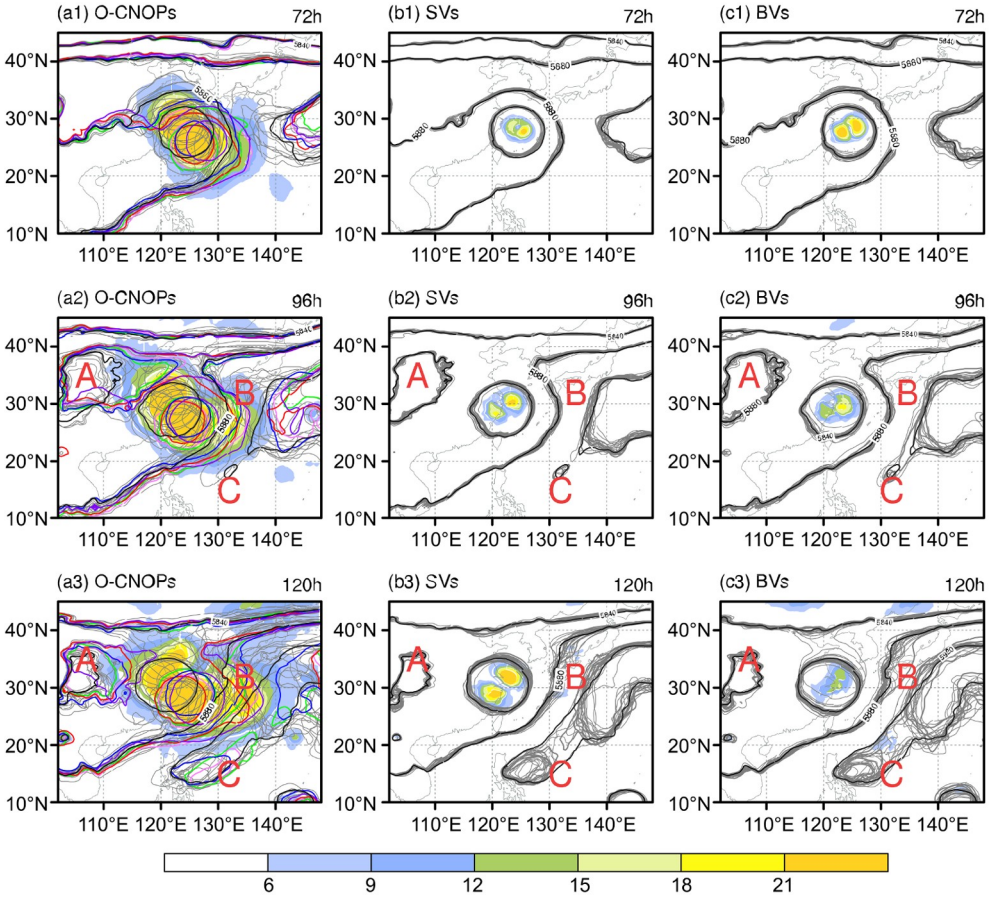

Figure 12 Ensemble spaghetti plots of 500 hPa geopotential height of 5920, 5880 and 5840 gpm (contours), along with their spreads (shaded; unit: gpm), made by the O-CNOPs, SVs, and BVs at lead times of 72 to 120 h for the three ensemble prediction systems. The black contours represent the control forecast, the colored contours represent the five O-CNOPs members that successfully predict the sharp northeastward turn of Khanun (2023), and the gray contours represent the remaining ensemble members.

However, the SVs and BVs ensembles show much less diversity in the intensity and location of the WPSH (see Figure 12b and Figure 12c), leading to a smaller spread in the steering flows surrounding the TC (see Figure 11b and Figure 11c). Therefore, the tracks of Khanun (2023) in both SVs and BVs ensembles exhibit smaller spreads around the control forecast, failing to cover the actual turning location and angle (see Figure 2). As discussed in Section 3.2, both SVs and BVs erroneously predict Khanun (2023) to make landfall on China's eastern coast before turning eastward with a much smaller angle compared to the best track. Conversely, the O-CNOPs ensemble adequately represents the uncertainty associated with the TC's sharp turn, providing a high probability of capturing the northeastward turn of Khanun (2023).

Let us now elucidate the dynamics through which O-CNOPs yield large ensemble spreads in terms of turning location and angle. Initially, Khanun (2023) is steered northwestward by the strong WPSH. At a lead time of about 48 h, the northern WPSH rapidly weakens and eventually splits into two ridges by around 96 h: a weak subtropical ridge to the west of TC (marked by A in Figure 12) and a subtropical ridge (the main body of the WPSH) to the east of TC (marked by B in Figure 12). The western ridge provides a southward steering flow that counteracts the northward steering flow from the eastern ridge (see Figure 11), causing the TC to slow down before its turn. During this stage, the O-CNOPs ensemble shows large spreads north of Khanun (2023), indicating the uncertainties in the intensity of the WPSH and the location of the eastern and western ridges (see Figure 12a2). These uncertainties may adequately interpret the probability for the strength of the northwestward steering flow and then the northwestward speed of TC movement. Furthermore, the movement speed before the TC turn may affect the farthest northwestward location that TC can reach, i.e., the turning location of Khanun (2023). In the control forecast, the TC track has a much higher northwestward speed than the best track, resulting in a northwestward-biased turning location relative to the observed turning location. This bias can partly be attributed to the rapid weakening and westward withdrawal of the western ridge in the control forecast, as depicted by the black contours in Figure

12. In contrast, the O-CNOPs ensemble, as shown above, presents a large spread in the TC movement speeds, thereby yielding a large spread in the turning location of Khanun (2023). Some ensemble members, particularly those with a stronger western ridge (represented by the colored contours in Figure 12a), accurately predict the actual turning location. Additionally, as an anticyclone develops on the southern side of TC (marked by C in Figure 12), the southwesterly flow in its northwestern portion strengthens and combines with the southerly flow in the western portion of the eastern ridge (see Figure 11). This interaction forces Khanun (2023) to turn sharply northeastward at a lead time of about 120 h. At this time, the O-CNOPs ensemble shows greater diversity in the intensity and location of the southern and eastern anticyclones, as evidenced by the large spread along the south-to-east portion of the TC (see Figure 12a3). This variability contributes to the large spreads in the relative magnitudes of the northern and western components of the steering flow surrounding TC (see Figure 11a5), and results in a broader spread in the TC moving direction after deflection as well as the turning angle of Khanun (2023). In the control forecast, the TC moves northward rather than northeastward as the best track at lead times of 120 to 144 h. This discrepancy is possibly due to an overestimation of the northward steering flow from an excessively strong eastern ridge and an underestimate of the northeastward steering flow from a relatively weak southern anticyclone. However, these O-CNOPs members with colored contours in Figure 12a, characterized by a stronger southern anticyclone and a much weaker eastern ridge than the control forecast, correct the turning angle of the control forecast, and then make the TC move northeastward after the turn.

In conclusion, the O-CNOPs can provide ensemble members that effectively represent the uncertainties in the surrounding steering flows that influence the TC turn through the dynamic interactions between the TC and the WPSH. This enables O-CNOPs to capture the sharp northeastward turn of Khanun (2023), while both SVs and BVs fail to do so.

4. Summary and discussion

The forecast of unusual TC track remains a challenge in operational forecasting. In this study, we examine the performance of O-CNOPs in improving ensemble forecasting skill for unusual TC tracks. Using the WRF model, we apply O-CNOPs, SVs and BVs to generate initial perturbations and conduct ensemble forecast experiments for the unusual tracks of five TC cases (i.e., Megi (2010), Tembin (2012), Hinnamnor (2022), Khanun (2023) and Saola (2023)), covering twenty-three forecast periods during which the TCs experienced sharp turns. Utilizing these forecasts, we first evaluate the probabilities of the ensemble members generated by O-CNOPs, BVs and SVs in capturing the sharp turns of TCs. The results reveal that O-CNOPs have a greater capacity to generate more ensemble members that reproduce the sharp turns of TCs at much longer lead times, thereby providing more valuable early warning information on the sharp turns of TC tracks. Furthermore, the ensemble mean forecasts generated by O-CNOPs demonstrate more stable improvements over the control forecasts in predicting TC turns. Results show that O-CNOPs outperform SVs and BVs in predicting the sharp turns of TCs, both in deterministic and probabilistic aspects.

Using Khanun (2023) as an example, this study explains why O-CNOPs outperform SVs and BVs in generating ensemble members that reproduce the sharp TC track turning. That is because O-CNOPs properly identify the energy-related sensitivity of TC movement in the middle to lower troposphere and the dynamics-related sensitivity in the annulus around Khanun (2023). The most unstable structures of O-CNOPs provide ensemble members that effectively depict the large uncertainties in the surrounding steering flow associated with the northeastward turn of Khanun (2023) through the dynamical interaction between Khanun (2023) and the WPSH, thereby capturing the location and angle of the sharp northeastward turn of TC. In contrast, both SVs and BVs fail to do so and miss its sharp northeastward turn. Moreover, the ensemble forecasts generated by O-CNOPs also provide a unique dataset for understanding the dynamical processes that may cause unusual TC movements and limit TC track predictability, offering a possible direction for reducing error sources through targeted observations or model improvements.

The results underscore the great potential of O-CNOPs in enhancing the forecasting reliability of unusual TC tracks. However, it is worth noting that the model resolution adopted in this study (30 km) is still too coarse for some TC cases. For example, all the ensemble forecasts generated by O-CNOPs, BVs and SVs have poor performance in forecasting the looping motion of Saola (2023). This limitation could be attributed to the inability of a 30-km resolution to properly resolve the small-scale TC structure and its interaction with the surrounding environment. Consequently, higher-resolution WRF simulations are needed to address such TC cases. One of the challenges in adopting higher resolutions is the significant computational cost associated with traditional optimization algorithms used to calculate O-CNOPs. Fortunately, recent research by Ma et al. (2025) proposed a parallel iterative method to efficiently calculate O-CNOPs. They demonstrated its high efficiency and effectiveness in ensemble forecasts using an idealized model. By applying this efficient algorithm to a higher-resolution WRF, we anticipate achieving skillful ensemble forecasts of TC tracks in real time. It is also hoped that the application of such an

efficient algorithm can be extended to convective-scale ensemble forecasts for TC intensity, TC-induced precipitation, and other high-impact weather systems.

Nowadays, some data assimilation schemes have been applied to naturally provide initial conditions for ensemble forecasts, such as the Ensemble Kalman Filter (EnKF). These schemes can provide good initial analysis fields and reflect the effect of observational distribution on initial uncertainties (Wang and Bishop, 2003; Ma et al., 2008; Feng et al., 2016). However, they often generate insufficient spread, leading to an underestimation of forecast uncertainties, which commonly requires an inflation coefficient to partially compensate for this limitation (Yang et al., 2015; Zheng and Zhu, 2016; Duan et al., 2019; Li and Zhao, 2022). This study only compares the O-CNOPs method with these traditional initial perturbation methods based on dynamical error growth theory (i.e., BVs and SVs). Future work will compare the performance of O-CNOPs and EnKF for ensemble forecasts of TC tracks. Besides initial errors, model errors also influence TC forecasts. The O-CNOPs method only considers the effect of initial uncertainties to generate ensemble forecasts. Although O-CNOPs achieve better reliability compared to traditional initial perturbation methods, the spread-skill relationship is still imperfect for measuring the reliability of the ensembles. For example, under the configuration determined by Zhang et al. (2023), O-CNOPs tend to overestimate the forecasting uncertainties of TC tracks. Duan et al. (2022) demonstrated that dynamically coordinated growth of initial and model perturbations helps produce ensembles with higher reliability when both initial and model errors are present in forecasts. Therefore, adopting combined modes of initial and model perturbations, such as the C-NFSVs proposed by Duan et al. (2022), is crucial for accounting for the combined effects of initial and model uncertainties in ensemble forecasts and thereby enhancing forecast reliability.

Acknowledgements *The authors appreciate the two anonymous reviewers for their insightful comments and suggestions. This work was jointly supported by the National Natural Science Foundation of China (Grant Nos. 41930971) and the International Partnership Program of the Chinese Academy of Sciences (Grant Nos. 060GJHZ2022061MI). The numerical experiments was supported by the National Key Scientific and Technological Infrastructure project "Earth System Numerical Simulation Facility" (EarthLab).*

Conflict of interest The authors declare no conflict of interest.

References

Birgin E G, Martínez J M, Raydan M. 2000. Nonmonotone spectral projected gradient methods on convex sets. SIAM J Optim, 10: 1196–1211

Chan J C L, Li K K. 2005. Ensemble forecasting of tropical cyclone motion using a barotropic model. Part III: Combining perturbations of the environment and the vortex. Meteorol Atmos Phys, 90: 109–126

Chen R, Zhang W, Wang X. 2020. Machine learning in tropical cyclone forecast modeling: A review. Atmosphere, 11: 676

Chen Y H, Sha S H, Lin C H, Hsiao L F, Huang C Y, Kuo H C. 2024. Performance evaluation of TGFS typhoon track forecasts over the western North Pacific with sensitivity tests on cumulus parameterization. Atmosphere, 15: 1075

Cheung K K W. 2001. A review of ensemble forecasting techniques with a focus on tropical cyclone forecasting. Meteorol Appl, 8: 315–332

Cheung K K W, Chan J C L. 1999. Ensemble forecasting of tropical cyclone motion using a barotropic model. Part I: Perturbations of the environment. Mon Weather Rev, 127: 1229–1243

Conroy A, Titley H, Rivett R, Feng X, Methven J, Hodges K, Brammer A, Burton A, Chakraborty P, Chen G, Cowan L, Dunion J, Sarkar A. 2023. Track forecast: Operational capability and new techniques-summary from the tenth international workshop on tropical cyclones (IWTC-10). Tropical Cyclone Res Rev, 12: 64–80

Dai G J, Wen Y R, Li Y. 2014. Statistical characteristics of tropical cyclone motion and sharp turning over northwestern Pacific (in Chinese). J Trop Meteorol, 30: 23–33

Diaconescu E P, Laprise R. 2012. Singular vectors in atmospheric sciences: A review. Earth-Sci Rev, 113: 161–175

Duan W S, Huo Z H. 2016. An approach to generating mutually independent initial perturbations for ensemble forecasts: Orthogonal conditional nonlinear optimal perturbations. J Atmos Sci, 73: 997–1014

Duan W S, Li X Q, Tian B. 2018. Towards optimal observational array for dealing with challenges of El Niño-Southern Oscillation predictions due to diversities of El Niño. Clim Dyn, 51: 3351–3368

Duan W S, Ma J J, Vannitsem S. 2022. An ensemble forecasting method for dealing with the combined effects of the initial and model errors and a potential deep learning implementation. Mon Weather Rev, 150: 2959–2976

Duan W S, Wang Y, Huo Z H, Zhou F F. 2019. Ensemble forecast methods for numerical weather forecast and climate prediction: Thinking and prospect (in Chinese). Clim Environ Res, 24: 396–406

Dube A, Ashrit R, Kumar S, Mamgain A. 2020. Improvements in tropical cyclone forecasting through ensemble prediction system at NCMRWF in India. Tropical Cyclone Res Rev, 9: 106–116

Feng J, Ding R Q, Li J P, Liu D Q. 2016. Comparison of nonlinear local Lyapunov vectors with bred vectors, random perturbations and ensemble transform Kalman filter strategies in a barotropic model. Adv Atmos Sci, 33: 1036–1046

Gong Y, Li Y, Zhang D L. 2018. A statistical study of unusual tracks of tropical cyclones near Taiwan Island. J Appl Meteorol Climatol, 57: 193–206

Huo Z H, Duan W S, Zhou F F. 2019. Ensemble forecasts of tropical cyclone track with orthogonal conditional nonlinear optimal perturbations. Adv Atmos Sci, 36: 231–247

Lang S T K, Leutbecher M, Jones S C. 2012. Impact of perturbation methods in the ECMWF ensemble prediction system on tropical cyclone forecasts. Q J R Meteorol Soc, 138: 2030–2046

Lei L, Ge Y, Tan Z M, Zhang Y, Chu K, Qiu X, Qian Q. 2022. Evaluation of a regional ensemble data assimilation system for typhoon prediction. Adv Atmos Sci, 39: 1816–1832

Li Y, Heming J, Torn R D, Lai S, Xu Y, Chen X. 2023. Unusual tracks: Statistical, controlling factors and model prediction. Tropical Cyclone Res Rev, 12: 309–322

Li Y, Zhao D. 2022. Climatology of tropical cyclone extreme rainfall over China from 1960 to 2019. Adv Atmos Sci, 39: 320–332

Liu L, Feng J, Ma L, Yang Y, Wu X, Wang C. 2024. Ensemble-based sensitivity analysis of track forecasts of typhoon In-fa (2021) without and with model errors in the ECMWF, NCEP, and CMA ensemble prediction systems. Atmos Res, 309: 107596

Lorenz E N. 1996. Predictability: A problem partly solved. Workshop on Predictability, Reading, United Kingdom, ECMWF, 1: 1–18

Ma J J, Duan W S, Liu Z M, Wang Y. 2025. A new method to calculate nonlinear optimal perturbations for ensemble forecasting. Adv Atmos Sci, 42: 952–967

Ma M, Peng M S, Li T, Wang L. 2022. Understanding the unusual track of

Typhoon Lionrock (2016). Weather Forecast, 37: 393–414
Ma X L, Xue J S, Lu W S. 2008. Preliminary study on ensemble transform Kalman filter-based initial perturbation scheme in GRAPES global ensemble prediction (in Chinese). Acta Meteorol Sin, 4: 526–536
Magnusson L, Doyle J D, Komaromi W A, Torn R D, Tang C K, Chan J C L, Yamaguchi M, Zhang F. 2019. Advances in understanding difficult cases of tropical cyclone track forecasts. Tropical Cyclone Res Rev, 8: 109–122
Miller W, Zhang D L. 2019. Understanding the unusual looping track of hurricane joaquin (2015) and its forecast errors. Mon Weather Rev, 147: 2231–2259
Miyachi T, Enomoto T. 2021. Tropical cyclone track forecasts using NCEP-GFS with initial conditions from three analyses. SOLA, 17: 140–144
Nie G Z, Xu Y L, Wang H P. 2025. Analysis of the characteristics and forecast difficulties of typhoon activities in the western North Pacific in 2023 (in Chinese). Meteorol Mon, 51: 369–381
Palmer T. 2019. The ECMWF ensemble prediction system: Looking back (more than) 25 years and projecting forward 25 years. Q J R Meteorol Soc, 145: 12–24
Pattanayak S, Mohanty U C. 2008. A comparative study on performance of MM5 and WRF models in simulation of tropical cyclones over Indian seas. Curr Sci, 95: 923–936
Puri K, Barkmeijer J, Palmer T N. 2001. Ensemble prediction of tropical cyclones using targeted diabatic singular vectors. Q J R Meteorol Soc, 127: 709–731
Qian Q F, Mao D Y. 2023. Evaluation of tropical cyclone track forecast performance of ECMWF and NCEP ensemble models from 2010 to 2019 (in Chinese). Meteorol Mon, 49: 224–234
Qian W, Du J, Ai Y, Leung J, Liu Y, Xu J. 2024. Anomaly-based variable models: Examples of unusual track and extreme precipitation of tropical cyclones. Meteorology, 3: 243–261
Skamarock W, Klemp J, Dudhia J, Gill D O, Barker D, Duda M G, Huang X Y, Huang W, Powers J G. 2008. A description of the advanced research WRF version 3. NCAR Technical Note, NCAR/TN-475+STR
Tang C K, Chan J C L, Yamaguchi M. 2021. Large tropical cyclone track forecast errors of global numerical weather prediction models in western North Pacific basin. Tropical Cyclone Res Rev, 10: 151–169
Thanh C, Tien T T, Chanh K Q. 2016. Application of breeding ensemble to tropical cyclone track forecasts using the Regional Atmospheric Modeling System (RAMS) model. Appl Math Model, 40: 8309–8325
Torn R D, Elless T J, Papin P P, Davis C A. 2018. Tropical cyclone track sensitivity in deformation steering flow. Mon Weather Rev, 146: 3183–3201
Toth Z, Kalnay E. 1993. Ensemble forecasting at NMC: The generation of perturbations. Bull Amer Meteorol Soc, 74: 2317–2330
Toth Z, Kalnay E. 1997. Ensemble forecasting at NCEP and the breeding method. Mon Weather Rev, 125: 3297–3319
Tseng J C H, Lai Y S. 2020. Perturbation structure and evolution in tropical cyclones Noul and Nepartak based on singular vectors. Tellus A-Dynamic Meteorol Oceanogr, 72: 1814589
Wang C X, Ni Y Q. 2011. Sensitivity experiments of impacting tropical cyclone track (in Chinese). Acta Meteorol Sin, 69: 757–769
Wang X, Bishop C H. 2003. A comparison of breeding and ensemble transform Kalman filter ensemble forecast schemes. J Atmos Sci, 60: 1140–1158
Xiang C, Ying L X, Shuan Z G, Qian W, Haiping W. 2022. Analysis of the characteristics and forecast difficulties of typhoon over the western North Pacific in 2021 (in Chinese). Meteorol Mon, 48: 1195–1208
Yamaguchi M, Majumdar S J. 2010. Using TIGGE data to diagnose initial perturbations and their growth for tropical cyclone ensemble forecasts. Mon Weather Rev, 138: 3634–3655
Yamaguchi M, Sakai R, Kyoda M, Komori T, Kadowaki T. 2009. Typhoon ensemble prediction system developed at the Japan Meteorological Agency. Mon Weather Rev, 137: 2592–2604
Yang S C, Kalnay E, Enomoto T. 2015. Ensemble singular vectors and their use as additive inflation in EnKF. Tellus A-Dynamic Meteorol Oceanogr, 67: 26536
Zhang X, Li Y, Zhang D L, Chen L. 2018. A 65-yr climatology of unusual tracks of tropical cyclones in the vicinity of China's coastal waters during 1949–2013. J Appl Meteorol Climatol, 57: 155–170
Zhang H, Duan W S, Zhang Y C. 2023. Using the orthogonal conditional nonlinear optimal perturbations approach to address the uncertainties of tropical cyclone track forecasts generated by the WRF model. Weather Forecast, 38: 1907–1933
Zheng F, Zhu J. 2016. Improved ensemble-mean forecasting of ENSO events by a zero-mean stochastic error model of an intermediate coupled model. Clim Dyn, 47: 3901–3915

(Editorial handling: Lili LEI)